ACS OMEGA

Open Access

http://pubs.acs.org/journal/acsodf

Article

Effect of Water on Effective Pore Structures for Medium-Rank Coal: Based on the Prefreezing Nitrogen Adsorption−Desorption Experiment

Zhixuan Li, Ke Wang,* Yi Lou, Peng Xia, Linjie Shao, Haiyang Hu, and Wei Gao

Cite This: *ACS Omega* 2023, 8, 42379−42389

Read Online

ACCESS | Metrics & More | Article Recommendations

ABSTRACT: Water is ubiquitous in coal reservoirs, and its distribution can have a remarkable influence on the effective pore space of methane. This study conducted the combination experiments of moisture equilibrium and prefreezing nitrogen adsorption−desorption to explore the adsorption behavior of water in coal pores and thus to reveal the distribution characteristics of water in pores with different scales as well as the influence of water on pore structures. The results showed that the adsorption mechanism of water vapor undergoes a transition from monolayer to multilayer to condensation with the increase in relative humidity (RH). The occurrence characteristics of adsorbed water in coal pores are controlled by the RH and pore size. When the RH is increased from 0 to 98%, the nitrogen adsorption capacity, specific surface area, and effective pore volume of the samples were all decreased significantly due to the different adsorption modes of water, which is more significant in pores with d < 10 nm. Additionally, the relative pressure corresponding to the branching position of the nitrogen adsorption-desorption curve will be changed with the increase in moisture content. Based on this, it is calculated that the adsorbed water will change the smoothness of the pore wall and the complexity of the pore structure.

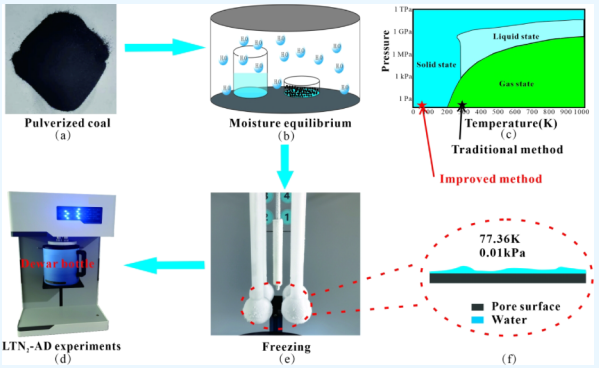

1. INTRODUCTION

Coalbed methane (CBM) is a new type of clean energy that can fill the energy gap in China.[1−3] Water and methane coexist in coal seams, and water has a significant effect on the pore structure and gas adsorption capacity of coal.[4−6] During the formation of coal, a large amount of water will be produced.[3,7] According to its storage form, water can also be divided into free water, adsorbed water, and chemically bound water.[8] Free water is stored in the fracture and macropores in a free state, while adsorbed water is retained in the microporous surface by physical adsorption. CBM is mainly divided into free gas and adsorbed gas, and its occurrence characteristics are similar to those of free water and adsorbed water. The adsorbed gas accounts for approximately 85% of the total gas in coal, while the specific proportion depends on the degree of metamorphism, burial depth of coal, and other factors.[9] The adsorbed water will compete with the gas for adsorption, which then affects the content of CBM.

As early as the 1970s, the occurrence characteristics of water in pores were studied by many scholars.[10] Zhao et al.[11] conducted a series of microscopic observation experiments on Weijiagou coal using field emission scanning electron microscopy (FESEM) and found that there were three main types of water occurrence states: crescent shape, fully filled shape, and annular shape. Chen et al.[12] found that adsorbed water has a significant effect on micropores smaller than 10 nm, while micropores smaller than 4 nm almost disappear in water-equilibrated coals, which is closely attributed to the water clusters and capillary water formed in the pore throats. Feng et al.[13] and Li et al.[14] analyzed the effect of water on the nanopore structure at different relative humidity (RH) levels using a nitrogen adsorption method and noted that the specific surface area of pores smaller than 10 nm could be reduced by up to 50−60%.

In addition, many scholars have also focused on the characteristics of gas occurrence in water-containing pores. Wang et al.[15] provided a schematic diagram of the occurrence characteristics of methane and water molecules in shale pores under different humidity conditions based on the principle of

Received: June 30, 2023
Revised: September 23, 2023
Accepted: September 29, 2023
Published: October 30, 2023

Table 1. Coal Sample Base Information

			mineral content (%)						proximate analysis (%)				
sample number	porosity (%)	R_o (%)	quartz	kaolinite	calcite	pyrite	diagonal chlorite	elysium	moisture	Ash	V_{ad}	V_{daf}	fixed carbon
A	2.67	1.03	35.6	53.9	7.5	3.0			0.97	25.91	27.15	37.00	46.67
B	2.94	1.35		33.0				67.0	1.19	10.00	23.32	26.22	66.40
C	2.80	1.11	56.7		24.4		18.9		1.16	17.80	26.56	32.69	55.33

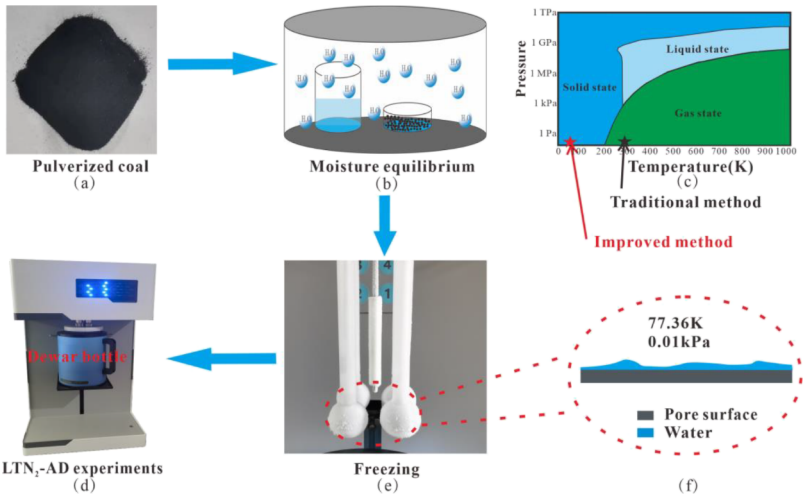

Figure 1. Experimental process of moisture equilibrium and prefreezing LTN_2-AD.

gas−water competitive adsorption. Moore,[3] Krooss et al.,[16] and Ma et al.[17] have shown that the adsorption capacity of methane decreases with increasing water content. Generally, the methane adsorption capacity of coal was decreased by 25% when the water content was increased by 1%. The reason for this phenomenon is that in the competitive adsorption between water molecules and methane, water molecules are preferentially adsorbed because coal contains hydrophilic functional groups such as carboxyl and hydroxyl groups, which easily form hydrogen bonds with H_2O molecules and occupy CH_4 adsorption sites, thus weakening the adsorption properties of coal for CH_4.[18] These findings suggested that additional methane gas can be adsorbed only in the larger pores of wet coal.

Scholars generally believe that the presence of water will reduce the methane storage capacity of coal, but most studies have focused on the interaction between water and methane, and less attention has been paid to the effect of water on the pore structure of coal, which is not conducive to the evaluation of CBM reserves. This study conducted the combination experiments of moisture equilibrium and prefreezing nitrogen adsorption−desorption to explore the adsorption behavior of water in the pores of medium-rank coal in the Shanjiaoshu mining area and thus to reveal the distribution characteristics of water in pores with different scales as well as the influence of water on pore structures. In addition, a new method was used to calculate the fractal dimensions of water-bearing pores. Finally, based on the adsorption characteristics of coal to water and the influence of water on pore structures, the characteristics of gas−water in coal pores are divided into four modes to better evaluate the influence of water on the coal pore structure. This review is organized as follows. Section 2 introduces sample information and experimental methods. Section 3 introduces the results of experiments of moisture equilibrium and prefreezing nitrogen adsorption−desorption. In Section 4, the experimental results are analyzed and discussed, Section 4.1 analyzes the effective pore size distribution law under different water content conditions; Section 4.2 analyzes the effect of water on the specific surface area and volume of pores; Section 4.3 uses a new method to calculate the fractal dimension of water-bearing pores; and Section 4.4 analyzes the occurrence characteristics of gas−water under different RH conditions.

2. SAMPLE INFORMATION AND EXPERIMENTAL METHODS

2.1. Sample Information. The coal samples A, B, and C used in this experiment were collected from the Shanjiaoshu mining area in Liupanshui, Guizhou, China, and basic information such as maturity, proximate components, and porosity of the coal samples is shown in Table 1. Based on the indicators such as volatile content, the coal samples in this study were all bituminous coal, and the coal samples A, B, and C are gas coal, fat coal, and fat coals, respectively. Based on the maximum vitrinite reflectance R_0 of the coal samples, it can be stated that the three coal samples in this test are medium-rank coals.

2.2. Experimental Instruments. In the low-temperature nitrogen gas adsorption−desorption experiments (LTN_2-AD), the coal samples were tested at a temperature of 77 K and a relative pressure of 0.001−0.99 using the JW-TB400 automatic specific surface area analyzer, which can analyze pore size characteristics in the range of 2−200 nm. Samples in each experiment had different RHs and a mass of approximately 1.5 g. We could reliably obtain the sample adsorption−desorption curve under different water content conditions and calculate the Brunauer−Emmet−Teller (BET) specific surface area and Barrett−Joyner−Halenda (BJH) pore volume of the samples by this instrument.[19,20]

2.3. Experimental Procedure. The complete experimental procedure is shown in Figure 1.

https://doi.org/10.1021/acsomega.3c04621
ACS Omega 2023, 8, 42379−42389

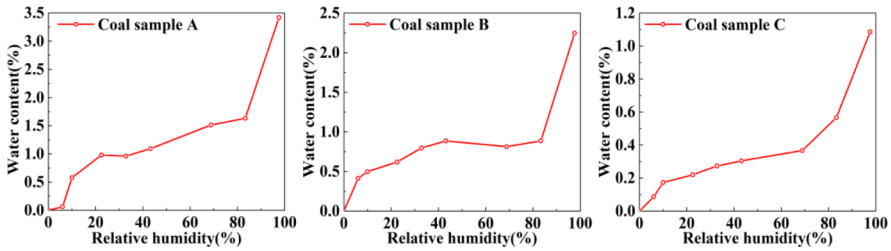

Figure 2. Water vapor adsorption curve.

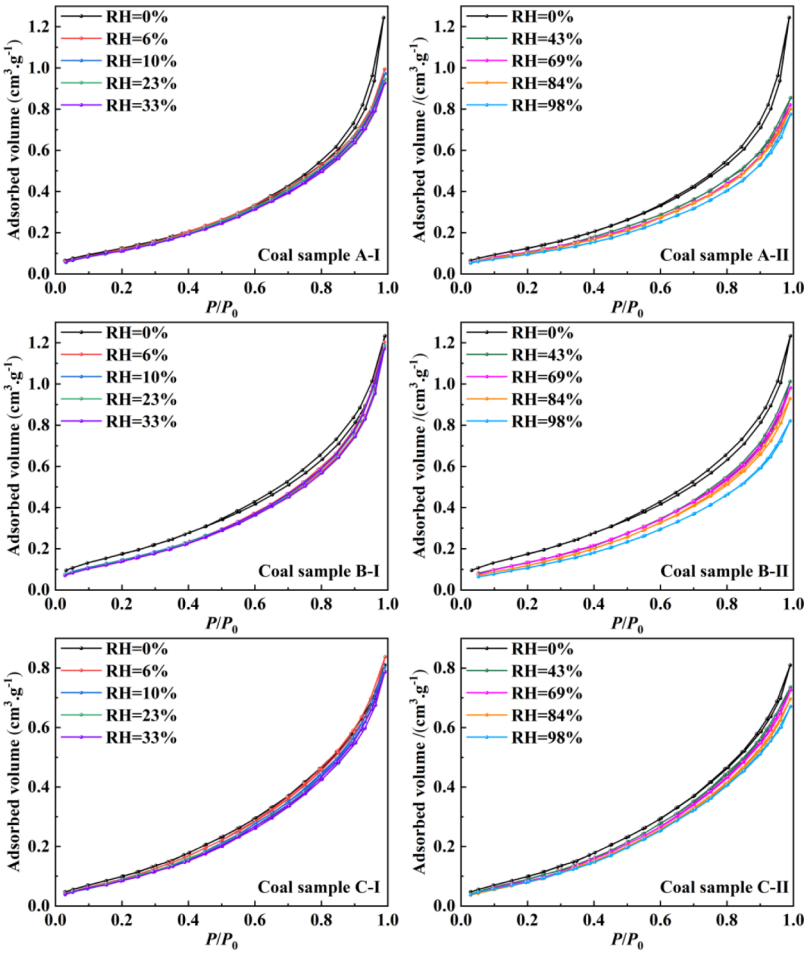

Figure 3. Adsorption−desorption curves obtained from the LTN_2-AD experiments.

First, the samples used in the experiment were obtained by crushing coal samples and passing them through 100−120 mesh coal sieves (Figure 1a). During the crushing process, the coal block was mainly broken along the cracks into particles that had little effect on the pore structure. Therefore, the pore structure of the coal particles in the experiment was representative of the coal seam pore structure.

Second, each coal powder sample was divided into nine portions of 1.5 g and was dried at 120 °C for 24 h to remove the moisture from the samples. Under room-temperature conditions (25 °C), eight groups of saturated salt solutions with RHs of 6% (BrLi), 10% ($ZnCl_2$), 23% (CH_3COOK), 33% ($MgCl_2$), 43% (K_2CO_3), 69% (KI), 84% (KCl), and 98% (K_2SO_4)[21] were prepared. Each solution together with an amount of pulverized coal was placed into a closed container and kept at a constant temperature (Figure 1b). After 48 h, samples were weighed at regular intervals until the mass change range of pulverized coal was reduced to less than 0.001 g, which marked the end of the moisture balance experiment.

Third, due to the traditional vacuuming step, the water in the coal pores (Figure 1f) will evaporate in the vacuum and normal temperature environment (Figure 1c), thus affecting the experimental results. In order to avoid this situation, the Dewar bottle was raised before the vacuuming step in the improved experiment, and the adsorbed water in the pores was frozen into a solid state (Figure 1e).

Finally, the low-temperature nitrogen adsorption−desorption experiment was carried out (Figure 1d).

3. RESULTS

3.1. Water Vapor Adsorption Characteristics of Coal.

According to the mass change during the moisture balance process, the moisture content of the coal sample is calculated by eq 1.[22]

https://doi.org/10.1021/acsomega.3c04621
ACS Omega 2023, 8, 42379−42389

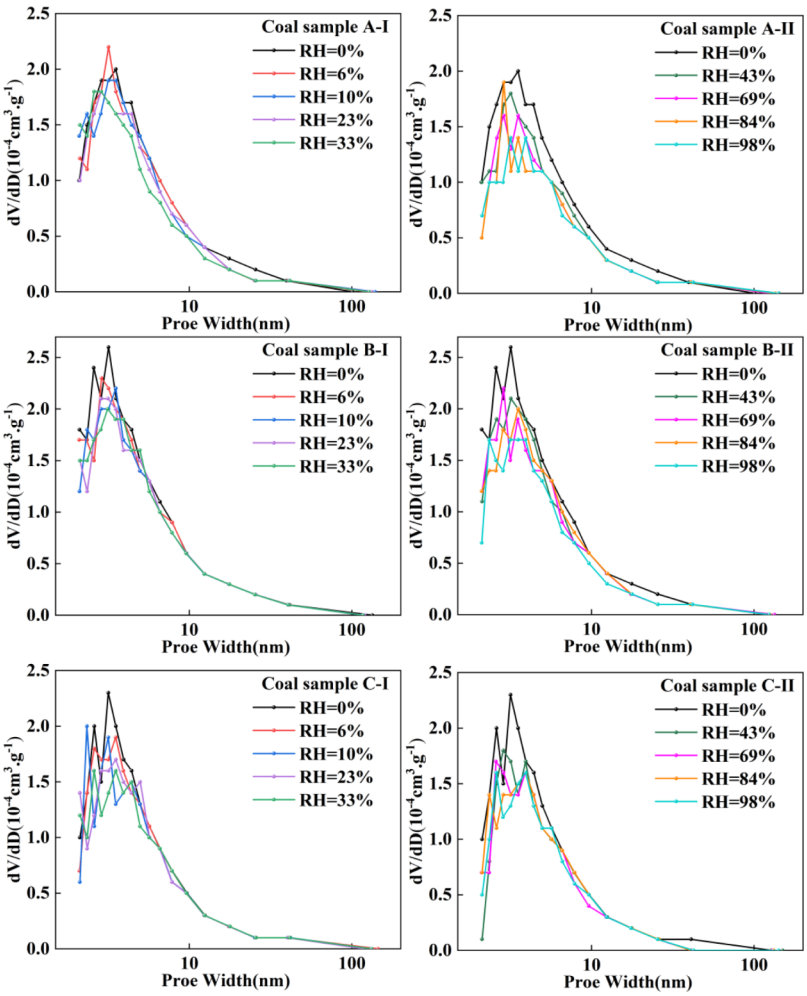

Figure 4. Characteristics of pore size distribution within different RHs.

$$M_{RH} = \frac{m_1 - m_0}{m_0} \quad (1)$$

where M_{RH} is the moisture content of the coal sample, m_0 is the sample mass in the dry state, g; and m_1 is the sample mass after equilibrium, g.

The moisture content variation curves of the three coal samples are shown in Figure 2, and the water adsorption curves are generally "S-shaped". Based on the morphology of the adsorption curve, the adsorption of water on coal samples can be roughly divided into three stages: (1) in the low-RH stage, water molecules quickly occupy the adsorption sites on the pore wall of the coal sample, resulting in a sharp increase in water content. This stage is dominated by monolayer adsorption of water molecules on the pore walls. The water content of the samples A, B, and C reached 0.98, 0.41, and 0.17%, respectively. (2) In the middle RH stage, the water content increases slowly. At this stage, water molecules are adsorbed in multiple layers on the pore wall surface. The water content of the three coal samples was increased to 1.63, 0.87, and 0.57%, respectively. (3) In the high-RH stage, multilayer adsorption led to an increase in the thickness of the water film, and the capillary coalescence of adsorbed water in tiny pores resulted in a sharp increase in water content. The water content of the three coal samples reached 3.42, 2.25, and 1.09%, respectively. Adsorbed water at this stage will induce the clay to expand and create new cracks, increasing the water absorption.[23] It is apparent that coal sample A has the largest water absorption and coal sample C has the smallest water absorption. The reason for the poorest adsorption capacity of coal sample C may be related to its low content of clay minerals. However, the water adsorption capacity of coal samples is also affected by factors such as oxygen-containing functional groups, porosity, maturity, and coal rank, which require further in-depth analysis.[24−26]

3.2. Nitrogen Adsorption−Desorption Curves. The morphology of the nitrogen adsorption−desorption curves reflects the pore structure characteristics of the samples to some extent.[27] The nitrogen adsorption−desorption curves of the coal rock samples under different RHs are shown in Figure 3. At low relative pressure P/P_0, the nitrogen adsorption capacity of the three groups of samples was increased slowly, while at relative pressure $P/P_0 > 0.8$, it was increased sharply. However, the adsorption saturation phenomenon did not occur, indicating the occurrence of capillary coalescence of nitrogen and the existence of many micropores and mesopores in the three groups of coal samples. The adsorption−desorption curves of the samples were reverse "S-shaped", with small hysteresis loops. Based on the pore structure reflected by the nitrogen adsorption−desorption forms,[28] the three groups of coal samples were mainly wedge-shaped pores and slit pores in the corresponding pore. Comparing the nitrogen adsorption−desorption curves of the same coal samples under different RH conditions, it was found that the curve configuration did not change significantly,

https://doi.org/10.1021/acsomega.3c04621
ACS Omega 2023, 8, 42379−42389

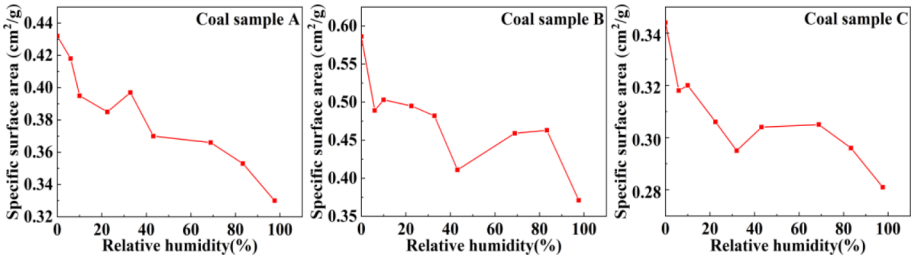

Figure 5. Specific surface area change graph with RH.

indicating that the effect of presorbed water on the pore structure was not significant within the experimental range.

It can be seen from the experimental principle of nitrogen adsorption−desorption that when the relative pressure P/P_0 was less than 0.2, the nitrogen adsorption−desorption curve rose faster and monolayer adsorption of nitrogen occurred on the pore wall at this stage. When the relative pressure P/P_0 was between 0.2 and 0.8, it rose slower and multilayer adsorption of nitrogen occurred. When the relative pressure P/P_0 was greater than 0.8, it rose faster and capillary coalescence of nitrogen occurred. The adsorption−desorption curves of the samples with different RHs were close to overlapping when P/P_0 of the coal sample was low, and only when P/P_0 was greater than 0.4, they showed significant differences. It indicated that the RH of coal sample A had a significant effect on the multilayer adsorption and capillary condensation of nitrogen in pores. In coal sample B, the relative pressure P/P_0 of the adsorption−desorption curves decreased significantly in the range 0−0.99 with the increase in RH. It indicated that the RH of coal sample B had a significant influence on the monolayer adsorption, multilayer adsorption, and capillary condensation of nitrogen on coal. In coal sample C, with the increase in RH, the adsorption−desorption curve decreased slightly, indicating that the RH of coal sample C had little effect on the adsorption of nitrogen.

In addition, the adsorption capacity of coal pore walls for nitrogen was influenced by the increase in RH of the coal sample. The maximum adsorption volume of nitrogen gradually decreased with the increase in RH as shown in Figure 3. The labels "A-I", "A-II", "B-I", "B-II", "C-I", and "C-II" are the denoted symbols of the nitrogen adsorption−desorption isotherms of coal samples at different humidity stages. For example, "A-I" represents the experimental results of sample A in the RH range of 0−33%, and "A-II" represents the experimental results of sample A in the RH range of 43−98%. As for coal sample A, the maximum adsorption volume of nitrogen in the dry condition was 1.24385 cm^3/g, and it was reduced to 0.77424 cm^3/g with an overall reduction of 37.75% when the RH was increased to 98%. As for coal sample B, the maximum adsorption volume of nitrogen in the dry condition was 1.19323 cm^3/g, and it was reduced to 0.8211 cm^3/g with an overall reduction of 31.19% when the RH was increased to 98%. As for coal sample C, the maximum adsorption volume of nitrogen in the dry state was 0.79782 cm^3/g, and it was reduced to 0.68043 cm^3/g with an overall reduction of 14.71% when the RH was increased to 98%. The changes of the maximum adsorption volume of nitrogen for sample C is the least when compared with samples A and B.

4. ANALYSIS AND DISCUSSION

4.1. Effective Pore Size Distribution Law under Different Water Content Conditions. The pore size distribution curves of coal samples after equilibrium at different RHs can be obtained by using the BJH equation according to the results of nitrogen adsorption−desorption curves.

As shown in Figure 4, the three groups of coal samples in the dry state have a unimodal distribution and mainly contain tiny pores of less than 10 nm. The pore diameters corresponding to the peaks of the coal samples A, B, and C were 3.53, 3.18, and 3.17 nm respectively, and the corresponding pore volumes were 0.19×10^{-3}, 0.26×10^{-3}, and 0.22×10^{-3} cm^3/g, respectively. With the increase in RH of coal samples, the pore size distribution curves with pore diameters smaller than 10 nm were decreased more than those with pore diameters larger than 10 nm. Compared with dry conditions, the differential pore volume of the coal samples was decreased with increasing RH. When the RH was 98%, the peak values of the pore volume of the coal samples A, B, and C were dropped to 0.15×10^{-3}, 0.17×10^{-3}, and 0.14×10^{-3} cm^3/g, respectively. With the increase of RH, the changes in the pore size distribution curves are not uniform, which indicates that the influence of water on the pore structure is complex.[29]

Regarding micropores, defined by IUPAC as the pores smaller than 2 nm, water adsorption is achieved through the filling of micropores, which differs from capillary condensation. It is evident that micropores cannot be analyzed using the BJH method; therefore, the impact of micropores (<2 nm) has not been addressed in this study.[30,31]

4.2. Effect of Water on the Specific Surface Area and Volume of Pores. *4.2.1. Variation of the Pore Specific Surface Area under Different RHs.* CBM is mainly stored in the nanoscale pores of coal in the state of adsorption. The content of the adsorption gas is related to the pore specific surface area. However, the water-containing state will hinder gas adsorption and affect the measured value of the specific surface. As shown in Figure 5, the BET specific surface area of the three groups of coal samples showed a decreasing trend with increasing RH. In sample A, the BET specific surface area was 0.432 cm^2/g under dry conditions and exhibited different degrees of decrease with the increase in RH. Specifically, when the RH was 98%, the BET specific surface area decreased to 0.33 cm^2/g (23.6% decrease). Similarly, for samples B and C, the BET specific surface area decreased from 0.5862 to 0.371 cm^2/g (36.7% decrease) and from 0.344 to 0.281 cm^2/g (18.3% decrease), respectively. These results indicated that the presence of moisture has a significant effect on the pore specific surface area of coal.

This study speculated about the reason why water affects the pore specific surface area based on the experimental results. When the RH was zero, nitrogen was directly adsorbed on the adsorption sites of the coal rock pore wall and the specific surface area was maximum at this point. The specific surface areas of the coal samples A, B, and C were 0.432, 0.586, and 0.344 cm^2/g, respectively. The declining trend of the specific surface area of

https://doi.org/10.1021/acsomega.3c04621
ACS Omega 2023, 8, 42379−42389

Table 2. BJH Pore Volume Variation of Coal Samples under Different RH Conditions

	coal sample A			coal sample B			coal sample C		
RH/%	$V_{BJH\text{-}Total}$/ (10^{-3}cm^3/g)	$V_{BJH\text{-}(d<10\,nm)}$/ ($10^{-3}$cm^3/g)	$V_{BJH\text{-}(d>10\,nm)}$/ ($10^{-3}$cm^3/g)	$V_{BJH\text{-}Total}$/ (10^{-3}cm^3/g)	$V_{BJH\text{-}(d<10\,nm)}$/ ($10^{-3}$cm^3/g)	$V_{BJH\text{-}(d>10\,nm)}$/ ($10^{-3}$cm^3/g)	$V_{BJH\text{-}Total}$/ (10^{-3}cm^3/g)	$V_{BJH\text{-}(d<10\,nm)}$/ ($10^{-3}$cm^3/g)	$V_{BJH\text{-}(d>10\,nm)}$/ ($10^{-3}$cm^3/g)
0	2.21	0.96	1.25	2.14	1.15	0.99	1.50	0.90	0.60
6	1.74	0.97	0.77	2.15	1.05	1.10	1.56	0.88	0.68
10	1.72	0.93	0.79	2.12	1.02	1.10	1.47	0.82	0.65
23	1.69	0.93	0.76	2.11	1.04	1.07	1.51	0.87	0.64
33	1.73	0.94	0.79	2.11	1.03	1.08	1.46	0.82	0.64
43	1.56	0.85	0.71	1.71	0.96	0.75	1.37	0.84	0.53
69	1.47	0.78	0.69	1.81	1.00	0.81	1.33	0.81	0.52
84	1.47	0.78	0.69	1.82	1.00	0.82	1.39	0.86	0.53
98	1.39	0.74	0.65	1.52	0.88	0.64	1.28	0.79	0.49

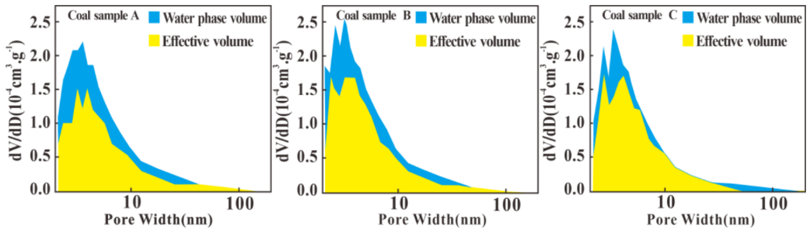

Figure 6. Effective pore distribution of coal samples at RH = 98%.

the pores with the changed RH can be divided into three stages. In the first stage (monolayer adsorption of water molecules), water molecules were adsorbed and covered the entire inner surface of the pores gradually to form water films. There are two modes, gas−solid adsorption and gas−liquid adsorption, in this stage. Since the adsorption capacity of water molecules on the inner surface of the pore is greater than that of nitrogen, with the increase of water molecules on the inner surface of the pores, nitrogen can only be adsorbed on the water film, resulting in a decrease in the amount of adsorbed nitrogen. This is the reason that the specific surface area of coal samples was decreased significantly in the low-RH stage. The second stage, namely, multilayer adsorption of water molecules, occurs when the RH is about 20−70%. The gas−liquid adsorption mode has not changed at this stage; the increase in RH almost does not affect the amount of adsorbed nitrogen. This is the reason why the specific surface area of coal samples at this stage was changed with a lest degree. In the third stage (capillary condensation clogging of pores), when the RH is approximately 70%, the thickness of the water film continues to increase. Owing to the limited pore size, the distance between the water films was decreased, and the capillary condensation of the water film blocked the pores under the forces of hydrogen bonding, causing a sharp decrease in the amount of adsorbed nitrogen.[32] This phenomenon initially occurs in small pores and then in larger pores.[33] This is confirmed in Figure 4, which shows the significant declining trend of the specific surface area in the high-RH stage.

4.2.2. Variation of Coal Pore Volume with Relative Humidity. The adsorbed gas content was mainly affected by the specific surface area, while the free gas content was mainly affected by the pore volume.[34] In this study, the pore volume under different RHs was calculated using BJH theory. In this study, the coal sample water absorption experiment was carried out at 298 K (25 °C), while the nitrogen adsorption−desorption experiment was carried out at 77 K (−196 °C); at this temperature, the liquid water films will turn into solid state, accompanied by volume expansion. To increase the thickness of the water films, the effective pore volume is decreased and the volume change of the water films caused by the expansion will change the density of water under the temperature conditions. Therefore, the expansion coefficient of the water film can be expressed as shown in eq 2:

$$\eta = \rho_w / \rho_s \quad (2)$$

Among them, ρ_w is the density of the liquid water film at 298 K, which is 0.996 g/cm^3,[35] and ρ_s is the density of the solid water film at 77 K, which is 0.941 g/cm^3.[35] Therefore, $\eta \approx 1.058$.

Therefore, it is necessary to introduce the parameter of expansion coefficient η to revise the calculation as shown in eq 3:

$$V_{BJH} = V_{BJH\text{-}EP} / \eta \quad (3)$$

where V_{BJH} is the real BJH pore volume and $V_{BJH\text{-}EP}$ is the experimental BJH pore volume.

According to eq 3, the modified $V_{BJH\text{-}Total}$ are shown in Table 2. Then, the Ходот decimal pore classification standard was used to analyze the influence of RH on the BJH pore volume of micropores (<10 nm) and large pores (>10 nm).[36]

The BJH pore volumes of the coal samples A, B, and C were 0.00221, 0.00214, and 0.00150 cm^3/g, respectively, among which the BJH pore volume of the coal sample A was the highest and that of coal sample C was the lowest. In the dry state, the total pore volume of the coal sample A mainly consisted of the pores with diameter (d) greater than 10 nm, while the total pore volume of the coal samples B and C mainly consisted of the pores with diameter (d) less than 10 nm (Table 2). With the increase in RH, the pore volumes of different pore diameters in the three groups of coal samples were decreased to different extents. When the RH reached 98%, the total BJH pore volume of coal samples A, B, and C decreased to 0.00139, 0.00152, and 0.00128 cm^3/g, respectively; the corresponding reduction degrees were 37.10, 28.97, and 14.67%, respectively.

From Figure 6, it is evident that the changes in the distribution of water volume and effective pore volume vary with different pore sizes when RH = 98%. It can be observed that water

https://doi.org/10.1021/acsomega.3c04621
ACS Omega 2023, 8, 42379−42389

Table 3. Variation of Fractal Dimension of Coal Samples under Different RH Conditions

	coal sample A			coal sample B			coal sample C		
RH/%	P^*	D_1	D_2	P^*	D_1	D_2	P^*	D_1	D_2
0	0.50	2.1504	2.6081	0.45	2.2024	2.6854	0.55	2.0090	2.7515
6	0.45	2.0701	2.6711	0.45	2.1478	2.6389	0.62	2.0097	2.6739
10	0.66	2.1008	2.7690	0.50	2.1811	2.6558	0.64	2.0049	2.7276
23	0.74	2.1331	2.7842	0.48	2.1546	2.6587	0.65	2.0069	2.7874
33	0.36	2.0627	2.6442	0.44	2.1478	2.6371	0.67	2.0073	2.7468
43	0.82	2.2136	2.8078	0.60	2.0978	2.7285	0.72	2.0162	2.8286
69	0.86	2.2590	2.8480	0.74	2.1699	2.7907	0.75	2.0371	2.8405
84	0.90	2.2438	2.8570	0.74	2.1845	2.7869	0.75	2.0616	2.8466
98	0.92	2.2917	2.8734	0.88	2.2263	2.8649	0.84	2.1033	2.8694

primarily penetrates into pores with d < 10 nm. This phenomenon is attributed to the fact that the small pores of coal samples are more susceptible to capillary condensation of water.[37] These pores do not completely disappear under the influence of capillary condensation, which is different from the result of former research studies that micropores will be vanished completely.[22] This is because coal pores possess some degree of hydrophobicity.[38], As for pores with d > 10 nm, water only occupies a small portion of the pore volume in the form of a water film owing to the low capillary pressure.[13]

4.3. Effect of Moisture Content on the Pore Fractal Dimension. The fractal dimension can quantitatively describe the complexity of the internal pore structure. Many scholars have found that the fractal dimension is related to the adsorption capacity of coal pores[39,40] and revealed a correlation between the surface area, pore size distribution, permeability, and pore system complexity with D_1 and D_2.[41−43] However, the acquirements are based on the measurement under dry conditions that are different from the real wet coalbed, and it is crucial to ascertain the potential impact of water on these measurements. Pfeifer.[44] proposed a method for calculating the fractal dimension based on the Frenkel−Halsey−Hill (FHH) model. The FHH model is shown in eq 4:

$$\ln V = C + K \ln\left(\ln \frac{P_0}{P}\right) \tag{4}$$

where V is the gas adsorption volume at the equilibrium pressure P, cm^3/g; C is a constant, dimensionless; the slope K is a constant related to the fractal dimension, dimensionless; P_0 is the saturated vapor pressure of the adsorbed gas, MPa; and P is the equilibrium pressure, MPa.

Pfeifer and Avnir[44] thought that the effective range of fractal dimension D was between 2 and 3. When D = 2, the surface is smooth, and the surface becomes rougher as D gets larger according to the relationship between D and K described by eq 5:

$$K + 3 = D \tag{5}$$

In this study, the relative pressure corresponding to the branch position in the nitrogen adsorption−desorption curve of the coal sample was named P^*. The adsorption−desorption curves of the samples (Figure 3) show two different gas adsorption mechanisms in the specific pressure ranges from zero to P^* and from P^* to one. At relative pressure $P/P_0 < P^*$, the hysteresis of the adsorption−desorption curve is not apparent, and the gas is mainly adsorbed on the surface of the coal body relied by the van der Waals force. When the relative pressure is $P/P_0 > P^*$, the hysteresis of the adsorption−desorption curve is significant, and the nitrogen is mainly adsorbed by the capillary condensation effect of the pores in the coal sample. In this study, the fractal dimensions were divided into D_1 and D_2. The fractal dimension D_1 (relative pressure less than P^*) reflects the phenomenon of adsorption and filling of nitrogen in the pores[44] and characterizes the roughness and complexity of pore walls.[45,46] The larger the value of D_1, the rougher the pore wall. The fractal dimension D_2 (relative pressure greater than P^*) mainly reflects the phenomenon of the capillary condensation process of nitrogen in the pores, which is used to characterize the complexity of the pore space and the irregularity of their structure.

Table 3 and Figure 7 show the fractal dimension of each group of coal samples with different RH conditions, among them, the red straight line is the fitting result related to D_2, and the blue straight line is the fitting result related to D_1. The fractal dimension D_1 decreased first and then increased with the increase in RH, indicating that the inner surface of the pores is smooth and then becomes rougher with the increase of water content. The reason for this phenomenon is that hollows and tiny pores will be filled by water molecules during monolayer adsorption,[37,47] which then makes the pore walls smoother. Then, as the RH increases, the uneven adsorption of water molecules on the pore wall leads to an increase in irregularity and disorder in the coal surface morphology. The fractal dimension D_2 increased with the increase in RH, indicating that the complexity of the pore structure is increased along with the increased moisture content within the range of the RHs. This result is consistent with the research result of Gu et al.[43] for water-bearing shale. First, the pores of coal have mixed wetting properties that contain oxygen-containing functional groups,[48,49] hydrophilic substances such as clay minerals and brittle minerals,[50] as well as hydrophobic substances such as organic matter and tar. Due to the different water absorption capabilities of these substances, the adsorption of water in the pores is uneven, which makes the pore structure complex in the water-containing state. Second, water exists in pores of different shapes and sizes within different states, and it is easy to form a "water bridge",[32,51] which further increases the complexity of the pore structure. Third, the ingress of water causes the expansion of clay minerals and also changes the pore structure.[47] Under the combined action of these factors, the pore structure of the coal samples becomes more complex.

4.4. Occurrence Characteristics of Gas−Water under Different RH Conditions. According to the schematic diagram of water adsorption in coal under different RH conditions proposed by Wu et al.,[24] this study combines the experimental results of water vapor adsorption and nitrogen adsorption−desorption to analyze the occurrence characteristics of water molecules and nitrogen molecules in coal pores (Figure 8).

https://doi.org/10.1021/acsomega.3c04621
ACS Omega 2023, 8, 42379−42389

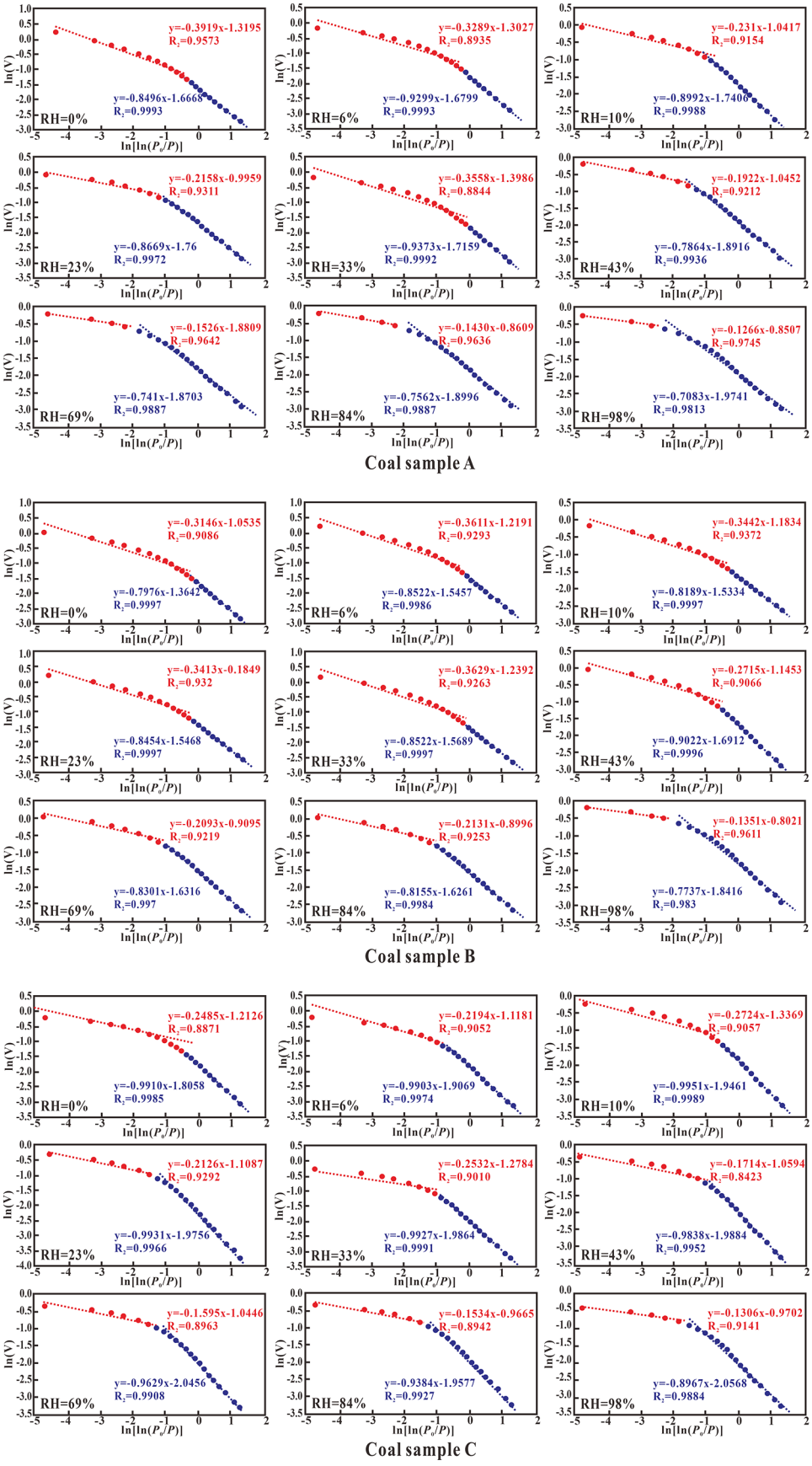

Figure 7. Fractal dimension of different coal samples at different RHs.

https://doi.org/10.1021/acsomega.3c04621
ACS Omega 2023, 8, 42379−42389

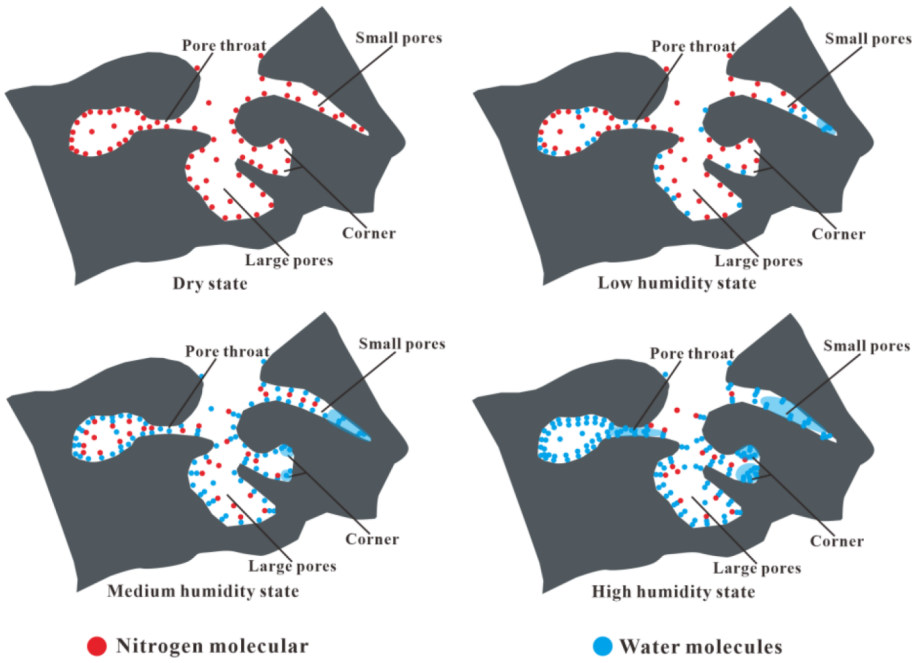

Figure 8. Gas−water occurrence patterns in coal pores under different RH conditions.

Type 1: In the dry state, nitrogen exists in the pore as an adsorbed and free state.

Type 2: In the low-RH condition, a part of the adsorption sites of nitrogen molecules on the pore wall is occupied by water molecules, some of the desorbed nitrogen molecules exist in the pore space, and the others are adsorbed on the water film. Because the main force between nitrogen and the pore wall is van der Waals, it tends to decrease when the condition becomes wetter. Therefore, the water film weakens the adsorption capacity of the pore wall for nitrogen. During this period, a small amount of capillary condensation of water emerges in the tiny pores.

Type 3: In the medium RH condition, the pore wall is covered by water molecules, water begins to exhibit in multi layers, and the water film gradually becomes thicker. In small pore corners, water films begin to gather together due to the close distance and condensation. During this period, the amount of capillary condensation of water in micropores is increased, along with the increased humidity.

Type 4: In the high-RH conditions, more and more small throats are filled by capillary condensation water, which then blocks the entrances of nitrogen and thus reduces the content of adsorbed gas.

5. CONCLUSIONS

(1) The occurrence characteristics of water in the pores change with the pore scale. Under certain RH conditions, water molecules mainly exist in the form of water condensation in the smaller pores when $d < 10$ nm and mainly exist in the form of water film on the wall of the larger pores when $d > 10$ nm.

(2) With the increase of water content, the nitrogen adsorption capacity, specific surface area, and pore volume of coal sample pores were all decreased. All of them decrease faster in the stages of single-layer adsorption and capillary condensation and slower in the stages of multilayer adsorption. When the RH was 98%, the specific surface areas of coal samples A, B, and C were decreased by 23.6, 36.7, and 18.3%, respectively, while the pore volumes were decreased by 37.10, 28.97, and 14.67%, respectively. Therefore, it is not an accurate result that the pore structure characteristics of coal samples are tested under dry conditions due to the actual conditions where the pores of coal contain different amounts of water.

(3) The branch point of the nitrogen adsorption−desorption curve will be affected by the water content. In this paper, the fractal dimension of water-bearing pores is calculated based on the changing relative pressure P^*. The results showed that the fractal dimension D_1 decreased initially and then increased, while the fractal dimension D_2 increased consistently, with the increase of water content, which indicated that the pore wall became smooth first and then rough; meanwhile, the pore structure became more complex as the water content increased.

AUTHOR INFORMATION

Corresponding Author

Ke Wang − *College of Resources and Environmental Engineering, Guizhou University, Guiyang 550025, China;* orcid.org/0000-0002-8294-2186; Email: 490260359@qq.com

Authors

Zhixuan Li − *College of Resources and Environmental Engineering, Guizhou University, Guiyang 550025, China;* orcid.org/0009-0008-7974-9511

Yi Lou − *Guizhou Panjiang Coalbed Methane Development and Utilization Company Limited, Guiyang 550081, China*

Peng Xia − *College of Resources and Environmental Engineering, Guizhou University, Guiyang 550025, China*

https://doi.org/10.1021/acsomega.3c04621
ACS Omega 2023, 8, 42379−42389

Linjie Shao − *Guizhou Panjiang Coalbed Methane Development and Utilization Company Limited, Guiyang 550081, China*

Haiyang Hu − *Guizhou Engineering Technology Research Center for Coalbed Methane and Shale Gas, Guiyang 550009, China*

Wei Gao − *Guizhou Engineering Technology Research Center for Coalbed Methane and Shale Gas, Guiyang 550009, China*

Complete contact information is available at: https://pubs.acs.org/10.1021/acsomega.3c04621

Notes

The authors declare no competing financial interest.

■ ACKNOWLEDGMENTS

The authors acknowledge the funds provided by Guizhou University (Number: 702825), the Science and Technology Program of Guizhou Province (Qian Science Foundation- ZK [2022] General 106, Qian Science Cooperation Project of Prospecting Strategy [2022] ZD001), National Natural Science Foundation Project of China (No. 42002166), and Geological Exploration Fund Project of Guizhou Province (No. 52000021 MGQSE7S7K6PRP).

■ REFERENCES

(1) Wang, X. Strategic consideration of China coal industry development during energy revolution and new normal of economic development. *China Coal* **2015**, *41* (04), 5−8.

(2) Wu, F.; Zhao, Z. The development status and future forecast of China's coal supply. *China Coal* **2018**, *44* (07), 5−8.

(3) Moore, T. A. Coalbed methane: A review. *Int. J. Coal Geol.* **2012**, *101* (1), 36−81.

(4) Merkel, A.; Gensterblum, Y.; Krooss, B. M.; Amann, A. Competitive sorption of CH4, CO2 and H2O on natural coals of different rank. *Int. J. Coal Geol.* **2015**, *150*, 181−192.

(5) Sun, J.; Xiao, X.; Cheng, P. Methane absorption of coal-measure shales with and without pore water from the Qinshui Basin, North China: Based on high-pressure methane absorption experiments. *Int. J. Coal Geol.* **2022**, *263*, No. 104116.

(6) Kang, N.; Chen, X.; Yang, H.; Zhao, S.; Qi, L. Effect of Different Placement Sequences of Water on the Methane Adsorption Properties of Coal. *ACS Omega* **2023**, *8* (7), 6689−6698.

(7) Su, X.; Lin, X. Coalbed methane geology. *China coal industry publishing house.* 2009.

(8) Cai, Y.; Zhai, C.; Yu, X.; Sun, Y.; Xu, J.; Zheng, Y.; Cong, Y.; Li, Y.; Chen, A.; Xu, H.; Wang, S.; Wu, X. Quantitative characterization of water transport and wetting patterns in coal using LF-NMR and FTIR techniques. *Fuel* **2023**, *350*, No. 128790.

(9) Chang, G.; Wang, Y.; Dong, T. An overview of research progress of adsorption and desorption of coal-Bed methane. *Petrochem. Ind. Technol.* **2015**, *22* (7), 125−126.

(10) Mahajan, O. P.; Walker, P. L. Water adsorption on coals. *Fuel* **1971**, *50* (3), 308−317.

(11) Zhao, Y.; Cao, S.; Li, Y.; Zhang, Z.; Guo, P.; Yang, H.; Zhang, S.; Pan, R. The occurrence state of moisture in coal and its influence model on pore seepage. *RSC Adv.* **2018**, *8* (10), 5420−5432.

(12) Chen, M.; Chen, X.; Wang, L.; Tian, F.; Yang, Y.; Zhang, X.; Yang, Y. Water adsorption characteristic and its impact on pore structure and methane adsorption of various rank coals. *Environ. Sci. Pollut. Res.* **2022**, *29* (20), 29870−29886.

(13) Feng, D.; Li, X.; Wang, X.; Li, J.; Si, J.; Zhang, T.; Li, P.; Chen, Y. Pore size distribution characteristic and methane sorption capacity of clay minerals under different water saturation. *J. China Coal Soc.* **2017**, *42* (9), 2402−2413.

(14) Li, J.; Li, X.; Wang, Z.; Xin, Y.; Han, J.; Si, J.; Sun, Z.; Wang, R. Effect of water distribution on methane adsorption capacity in shale clay. *Theor. Appl. Mech.* **2016**, *48* (5), 1217−1228.

(15) Wang, K.; Li, Z.; Ye, K.; Jiang, B.; Tan, Y.; Zhang, R. A new dynamic imbibition model for penny-shaped blind pores in shale gas well. *J. Nat. Gas Sci. Eng.* **2022**, *101*, No. 104553.

(16) Krooss, B. M.; Bergen, F. V.; Gensterblum, Y.; Siemons, N.; Pagnier, H. J. M.; David, P. High-pressure methane and carbon dioxide adsorption on dry and moisture-equilibrated pennsylvanian coals. *Int. J. Coal Geol.* **2002**, *51* (2), 69−92.

(17) Ma, X.; Song, Y.; Liu, S.; Jiang, L.; Hong, F. Experimental study on history of methane adsorption capacity of Carboniferous-Permian coal in Ordos Basin, China. *Fuel* **2016**, *184*, 10−17.

(18) Fu, X.; Zhang, D.; Xiang, W.; Lun, Z.; Zhao, C.; Wang, H.; Li, H. Influence of physicochemical properties of coals on pore morphology and methane adsorption: a perspective. *Chem. Ind. Eng. Prog.* **2019**, *38* (06), 2714−2725.

(19) Brunauer, S.; Emmett, P. H.; Teller, E. Adsorption of gases in multimolecular layers. *J. Am. Chem. Soc.* **1938**, *60* (2), 309−319.

(20) Barrett, E. P.; Joyner, L. G.; Halenda, P. P. The Determination of Pore Volume and Area Distributions in Porous Substances. I. Computations from Nitrogen Isotherms. *J. Am. Chem. Soc.* **1951**, *73* (1), 373−380.

(21) Astm, E. Standard practice for maintaining constant relative humidity by means of aqueous solutions. *ASTM Designation E* **2012**, *104*, 1.

(22) Feng, D.; Li, X.; Wang, X.; Li, J.; Sun, F.; Sun, Z.; Zhang, T.; Li, P.; Chen, Y.; Zhang, X. Water adsorption and its impact on the pore structure characteristics of shale clay. *Appl. Clay Sci.* **2018**, *155*, 126−138.

(23) Zolfaghari, A.; Dehghanpour, H.; Holyk, J. Water sorption behaviour of gas shales: I. Role of clays. *Int. J. Coal Geol.* **2017**, *179*, 130−138.

(24) Wu, H.; Yao, Y.; Liu, D. A modified Guggenheim-Anderson-Boer model for analyzing water sorption in coal. *Chem. Eng. J.* **2023**, *451*, No. 138760.

(25) Seemann, T.; Bertier, P.; Krooss, B. M.; Stanjek, H. Water vapour sorption on mudrocks. *Geol Soc. Spec. Pub.* **2017**, *454*, SP454.8.

(26) Ferrage, E.; Lanson, B.; Michot, L. J.; Robert, J. L. Hydration Properties and Interlayer Organization of Water and Ions in Synthetic Na-Smectite with Tetrahedral Layer Charge. Part 1. Results from X-ray Diffraction Profile Modeling. *J. Phys. Chem. C* **2012**, *114* (5), 4515−4526.

(27) Kuila, U.; Prasad, M. Specific surface area and pore-size distribution in clays and shales. *Geophys. Prospect.* **2013**, *61* (2), 341−362.

(28) Sun, M.; Yu, B.; Hu, Q.; Yang, R.; Zhang, Y.; Li, B. Pore connectivity and tracer migration of typical shales in south China. *Fuel* **2017**, *203*, 32−46.

(29) Xu, Y.; Chen, X.; Zhao, W.; Chen, P. Water vapor sorption properties on coals affected by hydrophilic inorganic minerals and pore fissures. *Fuel* **2022**, *324*, No. 124659.

(30) Li, J.; Li, X.; Wang, Z.; Li, Y.; Wu, K.; Shi, J.; Yang, L.; Feng, Dong; Zhang, T.; Yu, P. Water Distribution Characteristic and Effect on Methane Adsorption Capacity in Shale Clays. *Int. J. Coal Geol.* **2016**, *2016* (159), 135−154.

(31) Thommes, M. Physisorption of gases, with special reference to the evaluation of surface area and pore size distribution (IUPAC Technical Report). *Pure Appl. Chem.* **2016**, *87* (1), 25−25.

(32) Charrière, D.; Behra, P. Water sorption on coals. *J. Colloid Interface Sci.* **2010**, *344* (2), 460−467.

(33) Fan, Q.; Cheng, P.; Tian, H.; Gai, H.; Xiao, X. Distribution and occurrence of pore water and retained oil in nanopores of marine-terrestrial transitional shales during oil generation and expulsion: Implications from a thermal simulation experiment on shale plug samples. *Mar. Pet. Geol.* **2023**, *150*, No. 106125.

(34) An, F.; Cheng, Y.; Wu, D.; Wang, L. The effect of small micropores on methane adsorption of coals from Northern China. *Adsorption* **2013**, *19*, 83−90.

(35) Atkins, P. W.; Paula, J. C. D. *Physical Chemistr*; 7th ed.; Oxford University Press, 2002.
(36) Hodot, B. B. *Coal and Gas Outburst*; Song, S.; Wang, Y., translation; China Coal Publishing House: Beijing, 1966.
(37) Chen, M.; Chen, X.; Zhang, X.; Zhang, X.; Tian, F.; Sun, W.; Yang, Y.; Zhang, T. Experimental Study of the Pore Structure and Gas Desorption Characteristics of a Low-Rank Coal: Impact of Moisture. *ACS Omega* **2022**, *7* (42), 37293−37303.
(38) Song, B.; Zhai, X.; Ma, T.; Wang, B.; Hao, L.; Zhou, Y. Effect of water immersion on pore structure of bituminous coal with different metamorphic degrees. *Energy* **2023**, *274*, No. 127449.
(39) Li, Z.; Lin, B.; Gao, Y.; Cao, Z.; Cheng, Y.; Yu, J. Fractal analysis of pore characteristics and their impacts on methane adsorption of coals from Northern China. *Int. J. Oil, Gas Coal Technol.* **2015**, *10* (3), 306−324.
(40) Yao, Y.; Liu, D.; Tang, D.; Tang, S.; Huang, W. Fractal characterization of adsorption-pores of coals from North China: An investigation on CH4 adsorption capacity of coals. *Int. J. Coal Geol.* **2008**, *73* (1), 27−42.
(41) Chen, L.; Jiang, Z.; Jiang, S.; Liu, K.; Yang, W.; Tan, J.; Gao, F. Nanopore structure and fractal characteristics of lacustrine shale: implications for shale gas storage and production potential. *Nanomaterial* **2019**, *9* (3), 390.
(42) Wen, J.; Yan, S.; Zhen, J.; Mian, M.; Qing, L.; Lei, C.; Peng, W.; Feng, G.; He, H. Fractal characteristics of nano-pores in the Lower Silurian Longmaxi shales from the Upper Yangtze Platform, south China. *Mar. Pet. Geol.* **2016**, *78*, 88−98.
(43) Ke, G.; Zheng, N. Fractal dimension changes of shale pore structure and influence on mechanical properties, relative permeability under different hydration degree. *Environ. Earth Sci.* **2023**, *82*, 189.
(44) Pfeifer, P.; Avnir, D. Chemistry non-integral dimensions between two and three. *J. Chem. Phys.* **1983**, *79* (7), 3558−3565.
(45) Pfeifer, P.; Obert, M.; Cole, M. W. Fractal bet and FHH theories of adsorption: A comparative study. *Proc. R. Soc. A* **1990**, *423* (1864), 169−188.
(46) Peng, N.; He, S.; Hu, Q.; Zhang, B.; He, X.; Zhai, G.; He, C.; Yang, R. Organic nanopore structure and fractal characteristics of Wufeng and lower member of Longmaxi shales in southeastern Sichuan China. *Mar. Pet. Geol.* **2019**, *103*, 456−472.
(47) Ke, G.; Zheng, N.; Ying, K. Moisture influence on organic pore structure of shale. *Arab. J. Geosci.* **2021**, *14* (24), 2719.
(48) Hua, L.; Shi, T.; An, J.; Zuo, C.; Kai, S.; Yi, Z. Pore Characteristics and Fractal Dimension Analysis of Tectonic Coal and Primary-Structure Coal: A Case Study of Sanjia Coal Mine in Northern Guizhou. *ACS Omega* **2022**, *7* (31), 27300−27311.
(49) Zhi, X.; Xue, L.; Ke, Xi Study on the reactivity of oxygen-containing functional groups in coal with and without adsorbed water in low-temperature oxidation. *Fuel* **2021**, *304*, No. 121454.
(50) Xu, Y.; Chen, X.; Zhao, W.; Chen, P. Experimental and Numerical Simulation of Water Adsorption and Diffusion in Coals with Inorganic Minerals. *Energies* **2022**, *15*, 4321.
(51) Feng, W.; Yan, Y.; Zhi, W.; Qin, S.; Xue, Y. Effect of water occurrences on methane adsorption capacity of coal: A comparison between bituminous coal and anthracite coal. *Fuel* **2020**, 266.

https://doi.org/10.1021/acsomega.3c04621
ACS Omega 2023, 8, 42379−42389